

This is the author's accepted version of the manuscript.

The definitive version is published in *Journal of the Physical Society of Japan* 84 (2015)
054709, doi:10.7566/JPSJ.84.054709.

The final version published is available online at

<http://dx.doi.org/10.7566/JPSJ.84.054709>

©2015 The Physical Society of Japan

Possible Excitonic Phase of Graphite in the Quantum Limit State

Kazuto Akiba^{1*}, Atsushi Miyake¹, Hiroshi Yaguchi², Akira Matsuo¹, Koichi Kindo¹, and Masashi Tokunaga¹

¹*The Institute for Solid State Physics, The University of Tokyo, Kashiwa, Chiba 277-8581, Japan*

²*Department of Physics, Faculty of Science and Technology, Tokyo University of Science, Noda, Chiba 278-8510, Japan*

The in-plane resistivity, Hall resistivity, and magnetization of graphite were investigated in pulsed magnetic fields applied along the c -axis. The Hall resistivity approaches zero at approximately 53 T where the in-plane and out-of-plane resistivities steeply decrease. The differential magnetization also shows an anomaly at around this field with an amplitude similar to that of de Haas-van Alphen oscillations at lower fields. This transition field appears insensitive to disorder, but reduces with hole doping. These results suggest the realization of the quantum limit states above 53 T. As a plausible explanation for the observed gapped out-of-plane conduction above 53 T, the emergence of the excitonic BCS-like state in graphite is proposed.

1. Introduction

Graphite consists of stacked graphene layers along the c -axis and is known as a compensated semimetal having almost the same number of electron and hole carriers. The carrier densities are about $3 \times 10^{18} \text{ cm}^{-3}$ for both carriers, which is considerably lower than that in typical metals. Elongated Fermi surfaces are located along the H-K-H (H'-K'-H') points in the six edges of the hexagonal Brillouin zone. The electron-like Fermi surfaces exist near the K (K') points and the hole-like ones near the H (H') points. The band structure along the H-K-H (H'-K'-H') points is well explained by the Slonczewski-Weiss-McClure (SWM) model.^{1,2)}

In magnetic fields applied parallel to the c -axis, the band structure is quantized into Landau subbands, which show dispersion only along the c -axis. Owing to the small effective

*E-mail: k_akiba@issp.u-tokyo.ac.jp

mass of carriers in the basal plane, the quasi-quantum limit state, where only the lowest electron-like (Landau index of $n = 0$) and hole-like ($n = -1$) Landau subbands (each of them spin-split) cross the Fermi level, is realized at a moderate magnetic field of about 7.4 T.

The application of higher magnetic fields to the quasi-quantum limit state in graphite causes an abrupt increase in the in-plane resistivity above ~ 25 T.³⁾ Since the onset field strongly depends on temperature, this anomaly is ascribed to an electronic phase transition involving many-body effects.⁴⁾ A theoretical study by Yoshioka and Fukuyama (YF) suggested the formation of a charge-density-wave state caused by Fermi-surface nesting in the $n = 0$ spin-up ($0\uparrow$) subband. This theory reasonably reproduces the temperature dependence of the transition field.⁵⁾ Here, the direct Coulomb interaction was eliminated by assuming the antiphase charge modulation along the H-K-H and H'-K'-H' edges. According to this model, the transition temperature for the density-wave state T_c is given in the mean-field approximation as

$$k_B T_c = 4.53 E_F \frac{\cos^2(c_0 k_{F0\uparrow}/2)}{\cos(c_0 k_{F0\uparrow})} \exp\left(-\frac{2}{N_{0\uparrow}(E_F)u(\epsilon)}\right), \quad (1)$$

where E_F is the Fermi energy measured from the bottom of the Landau subbands, as shown in Fig. 1(a), and $N_{0\uparrow}(E_F)$ is the density of states at the E_F for the $0\uparrow$ subband. $k_{F0\uparrow}$ is the Fermi wavevector for this subband and c_0 is the lattice constant along the c -axis. $u(\epsilon)$ represents the relevant pairing interaction as a function of the dielectric constant (ϵ). In this formula, all the parameters E_F , $k_{F0\uparrow}$, $N_{0\uparrow}(E_F)$, and $u(\epsilon)$ depend on the magnetic field. On the other hand, Takahashi and Takada claimed that the spin-density-wave state, characterized by another nesting vector, becomes stable when the spatial separation of electrons along the H-K-H and H'-K'-H edges is taken into account.⁶⁾ Since there is no report on the direct experimental evidence of the nesting vector, the real nature in this field region remains as an open question.

Although Eq. (1) is given for a particular $2k_F$ instability, we remark that Eq. (1) has a similar functional form to the general BCS-type formula for mean-field-type pairing,⁷⁾

$$k_B T_c = 1.13 E_F \exp\left(-\frac{1}{N(E_F)V}\right), \quad (2)$$

where $N(E_F)$ is the density of states at the Fermi level and V is the relevant pairing interaction. When the Fermi energy approaches zero, T_c goes to zero in Eq. (2). Consequently, a density-wave state with T_c expressed by Eq. (2) is expected to exhibit a reentrant transition back to the normal state if the E_F of the relevant subband approaches zero in higher magnetic fields. Takada and Goto calculated the renormalized band structure taking into account self-energy effects, and found that the $0\uparrow$ and $-1\downarrow$ Landau subbands detach from the Fermi level almost

simultaneously at a crossing field of $\sim 53 \text{ T}^{8)}$ [see Fig. 1(b)].

In fact, measurements of the in-plane resistivity at magnetic fields of up to $\sim 55 \text{ T}$ obtained a clear indication of such a reentrant transition; the in-plane and out-of-plane resistivities show a sharp bend at a field close to the crossing field of $\sim 53 \text{ T}^{9,10)}$

Recently, Fauqué *et al.* have investigated the longitudinal resistivity (ρ_{zz}) at fields up to 80 T, and found an additional increase in ρ_{zz} above 53 T and a successive reduction in it above 75 T.¹¹⁾ The authors interpreted these anomalies as the sequential depopulation of Landau subbands, i.e., depopulation of the hole-like $-1\downarrow$ subband at 53 T and that of the electron-like $0\uparrow$ one at 75 T, and the emergence of a novel density-wave state in the intermediate field contrary to the preceding scenario. In this field region, the out-of-plane conduction exhibits gapped behavior, whereas the in-plane one (ρ_{xx}) remains metallic. This anomalous anisotropic conduction was explained with assuming parallel conduction through the chiral edge state, which is characteristic of the quantum Hall state.

To elucidate the true nature of the electronic states of graphite, studies of the Hall resistivity in high magnetic fields will be important. In highly oriented pyrolytic graphite (HOPG), Kopelevich *et al.* observed multiple anomalies in Hall resistivity in the field region between 16 and 43 T, and ascribed them to fractional quantum Hall plateaus.¹²⁾ They also reported the sign reversal of Hall resistivity at 43 T, and interpreted as the change of the majority carrier from electron to hole. Later, Kumar *et al.* reported that a similar sign reversal occurs even at room temperature,¹³⁾ suggesting the irrelevance of the sign reversal of Hall resistivity and the density-wave state in HOPG. In experiments on single crystalline Kish graphite up to 30 T, the absolute value of Hall resistivity steeply decreases in the density-wave state.¹⁴⁾ This result does not show any feature of fractional Hall plateaus at least up to 30 T. The Hall resistivity of single crystalline graphite above 30 T has not been reported yet.

To further understand the true electronic states of graphite in the field region over 30 T, we carried out simultaneous measurements of the in-plane resistivity and Hall resistivity up to 65 T and of the magnetization up to 75 T.

2. Experimental Methods

In this paper, we investigated the transport and magnetic properties of various types of graphite in high magnetic fields applied along the c -axis. We investigated three batches of Kish graphite (K01, K02, and K03), one super graphite (SG) obtained by graphitization of piled polyimide sheets, and one natural New York graphite (NY).

Since the in-plane chemical bonding is significantly stronger than the out-of-plane cou-

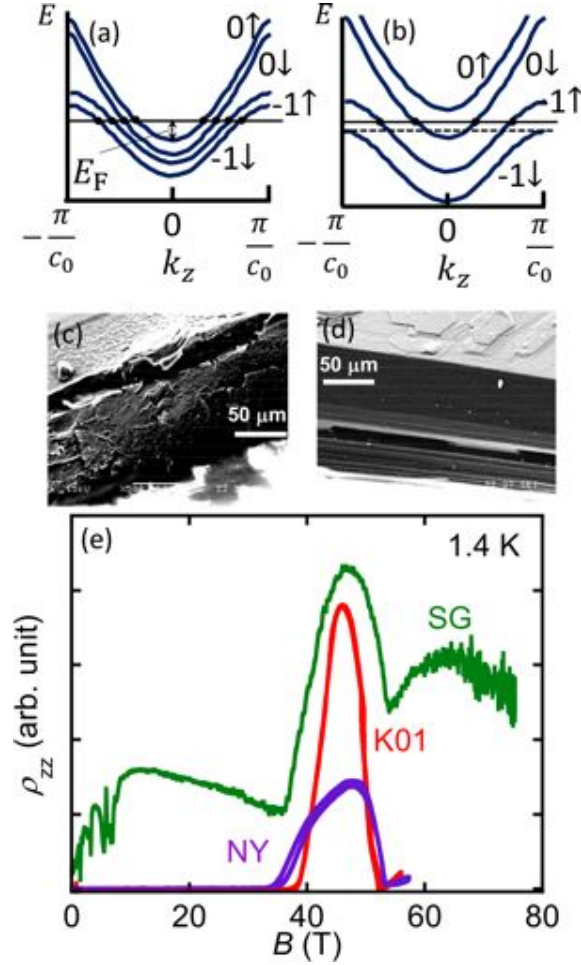


Fig. 1. (Color online) Schematic drawings of the band structures (a) below and (b) above 53 T calculated by TG.⁸⁾ The horizontal solid lines indicate the Fermi level of pristine graphite, while the dotted line in (b) indicates the Fermi level of the hole-doped one. Scanning electron microscope (SEM) images of the sample edges (c) cut by razor and (d) as-grown crystal of K01 samples. (e) Out-of-plane resistivities (ρ_{zz}) of as-grown K01, natural NY, and SG samples.

pling, mechanically shaped graphite usually has disordered edges, as shown in Fig. 1(c). Therefore, we mainly used as-grown crystals having clean edges, as shown in Fig. 1(d), to extract intrinsic transport properties. In addition, graphite is known as a highly anisotropic conductor showing nonlinear $I-V$ characteristics in the field-induced density-wave state.^{15,16)} To avoid the possible mixing of in-plane and out-of-plane conductions,^{17,18)} we used thin samples with the ratio of length to thickness of $\sim 50 - 100$ and formed electric contacts on their top surfaces for in-plane transport measurements. In this configuration, the possible partial cleavage in the sample might affect the evaluation of the absolute values of ρ_{xx} and ρ_{xy} . Thus, we do not discuss the quantitative aspect of the resistivity in this paper.

Figure 1(e) shows the out-of-plane resistivities (ρ_{zz}) of K01, NY, and SG. All the samples show an additional increase in ρ_{zz} above 53 T, as reported previously.^{9,11)} Therefore, we regard this increase as intrinsic in graphite.

The in-plane (ρ_{xx}) and Hall resistivity (ρ_{xy}) of the samples were measured simultaneously by a five-probe method using the numerical lock-in technique¹⁹⁾ at a frequency of 100 or 200 kHz. Epo-tek H20E silver epoxy and 30- μm -thick gold wires were used to form electrical contacts. Magnetization (M) was measured by an induction method using two pickup coils placed coaxially. To achieve a large signal-to-noise ratio in the magnetization measurement, the crystals of K01 were piled up with their c -axis aligned, as shown in the inset of Fig. 2(a). Magnetic fields were applied along the c -axis throughout the entire measurements.

Pulsed high magnetic fields were generated using nondestructive magnets installed at The Institute for Solid State Physics at The University of Tokyo. For magnetotransport measurements, magnetic fields up to 56 and 65 T (pulse durations of 36 and 4 ms, respectively) were generated using bipolar pulse magnets, which can generate both positive and negative fields. Mixing of the ρ_{xx} component into the nominal ρ_{xy} signal was eliminated by subtracting the data for different field polarities. Magnetization and some of ρ_{zz} were measured up to 75 T using a unipolar pulse magnet with a duration of 4 ms.

3. Results and Discussion

Figure 2(a) shows the field dependence of the magnetization (M) of K01. Monotonic sub-linear diamagnetism is observed up to 74 T. Figure 2(b) shows the differential magnetization dM/dH obtained by averaging seven data sets acquired under repeated experiments up to 62 T. The dM/dH curve up to 11 T is shown in the inset of Fig. 2(b). Oscillations in dM/dH observed in the region up to 7.4 T correspond to the de Haas-van Alphen (dHvA) effect, indicating that all subbands except for $n = 0$ and -1 detach from the Fermi level at fields below 7.4 T. In the main panel, we can hardly identify the anomaly at the transition field α shown below. On the other hand, a nonmonotonic change was observed at approximately 53 T.

Figure 3(a) shows the in-plane resistivity ρ_{xx} of K01 at various temperatures between 1.3 and 4.2 K. Shubnikov-de Haas oscillations are observed at magnetic fields below 7.4 T. At magnetic fields above 7.4 T, the observed abrupt increase and steep decrease in ρ_{xx} (marked with α and α') have been regarded as the emergence and collapse of the density-wave state, respectively. The critical field of the α transition shows a strong temperature dependence, indicating the importance of the many-body effect. On the other hand, the critical field of the

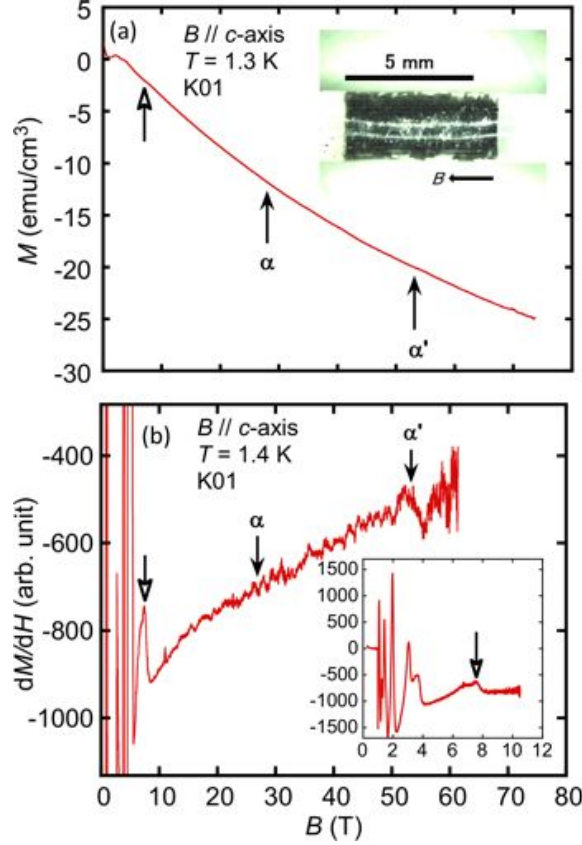


Fig. 2. (Color online) (a) Field dependence of magnetization of K01 sample up to 74 T at 1.3 K. The inset shows a picture of the sample used for the magnetization measurements. (b) Field dependence of differential magnetization of K01 up to 62 T. α and α' indicate the fields where the in-plane resistivity shows anomalies, while the open arrow indicates the field at which graphite goes into a quasi-quantum limit state. The inset shows the differential magnetization in the low-field region.

α' transition shows a rather weak temperature dependence as reported previously.⁹⁾ The other anomaly seen between α and α' pointed out in the previous reports^{9,20)} (which is referred to as the β anomaly below) is small in ρ_{xx} . We observed a clear β anomaly for the relatively thick samples (not shown). This geometrical effect implies that the β anomaly might be the superposition of the out-of-plane resistivity. We will not go into details about the β anomaly in this paper. The ρ_{xx} above 53 T decreases with decreasing temperature, in contrast to the gapped behavior in ρ_{zz} , as reported previously.¹¹⁾

Figure 3(b) shows the field dependence of the Hall resistivity ρ_{xy} at temperatures between 1.3 and 4.2 K. Shubnikov-de Haas oscillations are also observed at ρ_{xy} below 7.4 T. At magnetic fields above 7.4 T, an anomaly is clearly observed at α , but is less pronounced than that at ρ_{xx} . Some readers might be concerned with the relevance of this anomaly to the quantum Hall plateau. Since the normalized Hall resistivity per single graphite layer at α varies from

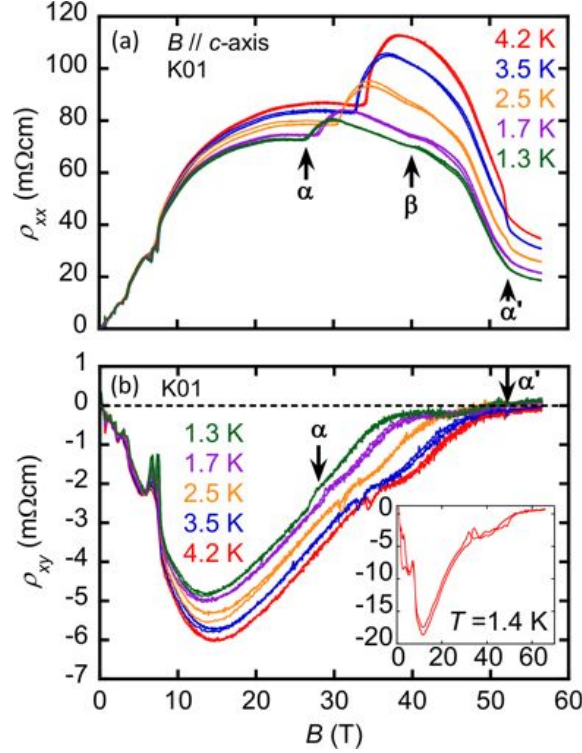


Fig. 3. (Color online) (a) In-plane resistivity and (b) Hall resistivity of K01 sample at various temperatures as functions of magnetic field applied along the c -axis. The inset of (b) shows the Hall resistivity up to 65 T at 1.4 K. The result shown in the inset was obtained for a different piece of K01 from that in the main panel.

sample to sample in the other sets of experiments on K01, we consider that this plateaulike anomaly at approximately $\rho_{xy} \sim -2$ mΩ cm is not related to the quantum Hall plateau. Fractional plateau-like structures, which have been reported on HOPG,¹²⁾ were not observed in this measurement. We also observed that ρ_{xy} gradually approaches zero as the applied field approaches 53 T. As shown in the inset of Fig. 3(b), ρ_{xy} remains almost zero even deeply in the high-field state between 53 and 74 T.

Figure 4 shows the field dependence of the conductivities σ_{xx} and σ_{xy} of K01. The σ_{xx} and σ_{xy} were obtained from the in-plane resistivity ρ_{xx} and the Hall resistivity ρ_{xy} using the following relationship:

$$\sigma_{xx} = \frac{\rho_{xx}}{\rho_{xx}^2 + \rho_{xy}^2}, \quad (3)$$

$$\sigma_{xy} = -\frac{\rho_{xy}}{\rho_{xx}^2 + \rho_{xy}^2}. \quad (4)$$

In high magnetic fields, the imbalance between the carrier densities of electrons (n_e) and holes

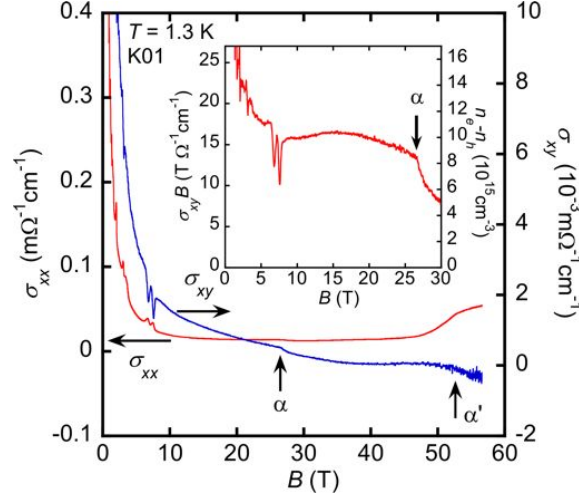


Fig. 4. (Color online) Field dependence of conductivities σ_{xx} (red) and σ_{xy} (blue) of K01 sample at 1.3 K. The inset shows the field dependence of $\sigma_{xy}B$ up to 30 T at 1.3 K. The scale on the right side of the inset gives a difference between electron and hole densities.

(n_h) is deduced within the framework of a semiclassical simple two-carrier model as follows:

$$n_e - n_h = \frac{\sigma_{xy}B}{e}. \quad (5)$$

The field dependence of $\sigma_{xy}B$ and the estimated imbalance are shown in the inset of Fig. 4. $\sigma_{xy}B$ is nearly constant in the field region between 8 and 15 T, then shows a slight decrease between 15 and 25 T. This reduction has been ascribed to the effect of magnetic freeze-out, which diminishes carriers provided by ionized impurities.²¹⁾ As shown in the inset of Fig. 4, $\sigma_{xy}B$ shows a marked decrease at α . As mentioned above, Uji *et al.*¹⁴⁾ ascribed this anomaly to the opening of a gap in the electron-like subband, which leads to the sign reversal of the Hall resistivity at higher fields. Contrary to this expectation, no apparent sign reversal was observed in our measurements up to 65 T. To clarify whether these features are intrinsic in graphite, we measured ρ_{xx} and ρ_{xy} in various types of graphite [Figs. 5(a) and 5(b)]. At ρ_{xx} , only the α transition field of SG is clearly higher than those of the other samples. The details of this difference will be discussed later. The ρ_{xy} values of K01, K02, K03, and SG are negative, whereas only natural NY shows a positive Hall resistivity. Regardless of its sign, ρ_{xy} approaches zero at the α' transition in all the samples, suggesting that it is intrinsic in graphite. No quantum-Hall plateau-like structure was observed in any sample.

Figure 5(c) shows the field dependence of the transition temperature for α (T_α). According to the BCS-like formula in Eq. (2), and assuming the increase in $N(E_F)$ in proportion to the magnetic field and ignoring the field dependences of E_F and V , Eq. (2) is rewritten in the

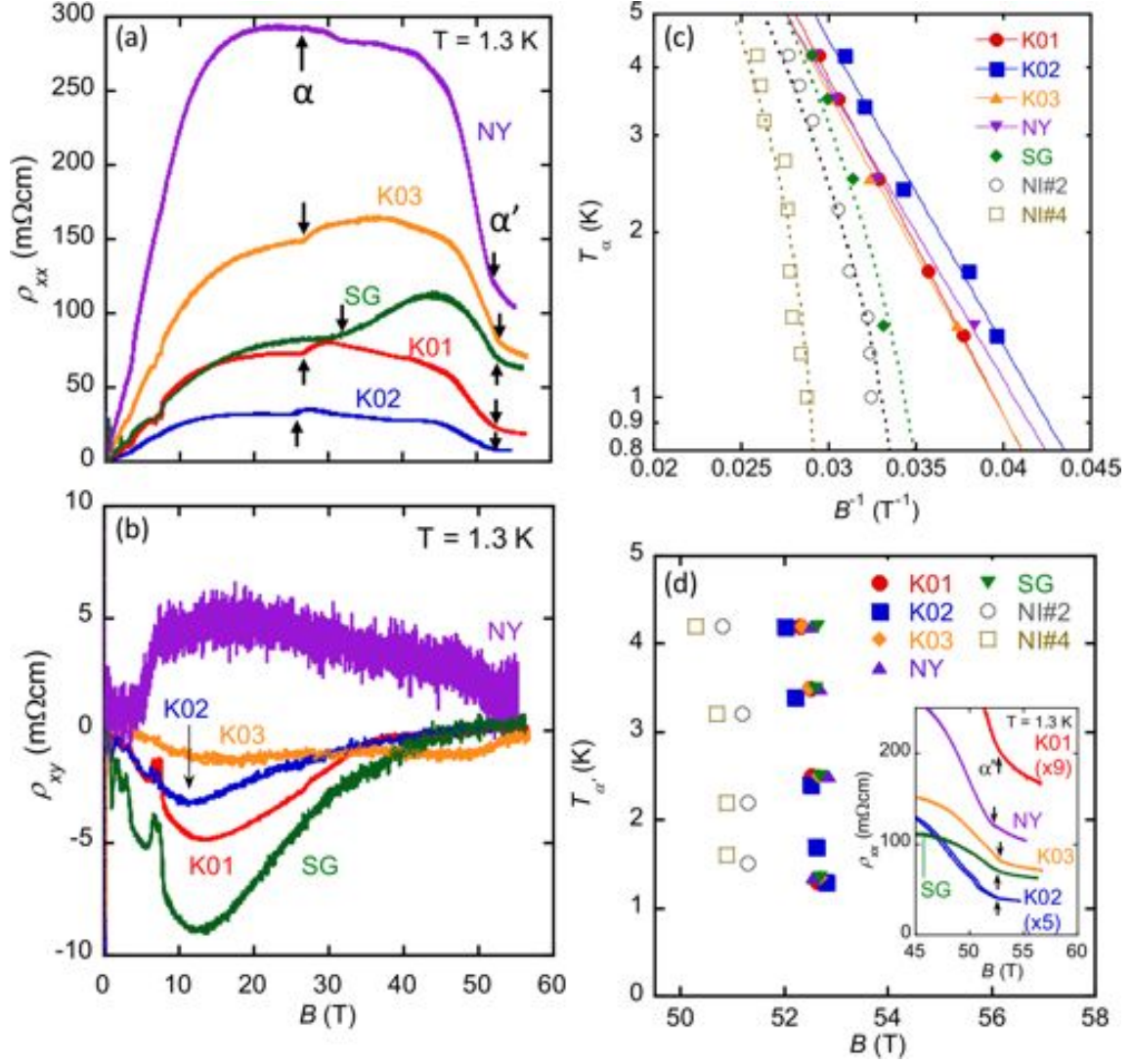


Fig. 5. (Color online) (a) In-plane resistivity ρ_{xx} and (b) Hall resistivity ρ_{xy} of five different samples at 1.3 K. (c) Field dependence of α transition temperature T_α as a function of inversed field. The open circles and squares represent the reported results of Kish graphite irradiated with fast neutrons for two (NI#2) and four (NI#4) hours, respectively.²²⁾ (d) Field dependence of α' transition temperature $T_{\alpha'}$ of five different pristine and two irradiated²³⁾ graphite samples. NI#2 and NI#4 are irradiated with the first neutron under the same condition, but different pieces from those in (c). The inset shows an enlarged view of (a) at around the α' transition field.

simpler form

$$T_\alpha = T^* \exp\left(-\frac{B^*}{B}\right), \quad (6)$$

where T^* and B^* are constants.⁴⁾ This formula gives a linear relationship between $\ln T_\alpha$ and the inversed field. The solid lines in Fig. 5(c) represent fitting curves for K01, K02, K03, and NY obtained using Eq. (6) with the parameters T^* and B^* as listed in Table I. Here, T^* and B^* simply modify the scales of vertical and horizontal axes, respectively. In our samples,

Table I. List of samples investigated in this report. T^* , B^* , and τ are fitting parameters in Eqs. (6) and (7).

sample	measured quantity	T^* (K)	B^* (T)	τ ($\times 10^{-12}$ s)	paper
K01 (Kish graphite)	$\rho_{xx}, \rho_{xy}, \rho_{zz}, M$	290	144	-	this work
K02 (Kish graphite)	ρ_{xx}, ρ_{xy}	270	136	-	this work
K03 (Kish graphite)	ρ_{xx}, ρ_{xy}	257	142	-	this work
NY (natural graphite)	$\rho_{xx}, \rho_{xy}, \rho_{zz}$	192	131	-	this work
SG (super graphite)	$\rho_{xx}, \rho_{xy}, \rho_{zz}$	270	136	4.5	this work
NI#2 (Kish graphite)	ρ_{xx}	191	128	3.9	Refs. 22 and 23
NI#4 (Kish graphite)	ρ_{xx}	191	128	2.0	Refs. 22 and 23

only the SG exhibits an nonlinear phase boundary that cannot be reproduced using Eq. (6). A similar discrepancy was also observed in neutron-irradiated graphite.²²⁾ Neutron irradiation to graphite is known to introduce lattice defects that act as acceptors, and hence, dope hole carriers. The reported field dependence of T_α of the neutron-irradiated Kish graphite is also shown in Fig. 5(c).²²⁾ The results for irradiated samples significantly deviate from that of Eq. (6) similar to the cases of SG. Yaguchi *et al.* explained the qualitative difference in the transition temperature with the introduction of the pair breaking effect on density-waves caused by charged impurities,²²⁾ similar to the arguments on different types of graphite below 1 K.²⁴⁾ In the mean-field form, the transition temperature reduced by the pair breaking effect (T_α^{PB}) is expressed as²⁴⁾

$$\ln\left(\frac{T_\alpha^{\text{PB}}}{T_\alpha}\right) = \psi\left(\frac{1}{2}\right) - \psi\left(\frac{1}{2} + \frac{\hbar}{2\pi k_B T_\alpha^{\text{PB}} \tau}\right). \quad (7)$$

$\psi(x)$ is the digamma function, T_α is the transition temperature without the pair breaking effect, which is given by Eq. (6), and τ is the relaxation time of pair breaking. The deviation from the functional form of Eq. (6) seen in the neutron-irradiated Kish graphite is well reproduced by Eq. (7), as shown in Fig. 5(c). Apparently, Eq. (7) also accounts for the reduction in T_α seen in SG. By using the values of $T^* = 270$ K and $B^* = 136$ T taken from those in the K02, the phase boundary of SG can be reasonably reproduced with $\tau = 4.5 \times 10^{-12}$ s, as shown by the dotted line in Fig. 5(c). Although the microscopic origin is unclear, the T_α of the SG is significantly affected by the pair breaking effect compared with those of the other four samples.

Although the T_α of SG shows a trace similar to those of neutron-irradiated samples, the transition temperature for α' ($T_{\alpha'}$) is significantly different. The $T_{\alpha'}$ values of all the samples

are plotted as a function of B in Fig. 5(d). The five pristine samples show almost similar boundaries, whereas the neutron-irradiated ones, quoted from the literature,²³⁾ show transitions at smaller fields. We consider that the reduction in the transition field at α' at a given temperature is not caused by the pair breaking effect because the observed reduction in that of SG is almost the same as those of the pristine Kish samples. The neutron-irradiated samples are known to have holes on the order of 10^{18} cm^{-3} , which is a hundred times larger than the charge imbalance for the pristine samples. Therefore, the reduction in the reentrant transition field at α' in irradiated samples can be caused by hole doping rather than pair breaking.

Let us discuss the transition at α' in the following. Firstly, since the differential magnetization shows an anomaly at approximately 53 T in the same order of magnitude as those in the dHvA oscillations at low fields (open arrows in Fig. 2), we regard this anomaly as the feature of the depopulation of the Landau subband. Within the accuracy of these measurements, however, we cannot determine the number of depopulated subbands at ~ 53 T.

To consider the number of populated Landau subbands above 53 T, we discuss the result of Hall resistivity beyond the simple two-carrier model. For a more precise argument, we have to calculate the in-plane and Hall conductivities using the Kubo formula

$$\sigma_{xy} = \frac{\hbar}{i} \sum_{\substack{nk\sigma \\ E_n < \epsilon_F < E_{n+1}}} \frac{\langle n | \hat{j}_x | n+1 \rangle \langle n+1 | \hat{j}_y | n \rangle - \langle n+1 | \hat{j}_x | n \rangle \langle n | \hat{j}_y | n+1 \rangle}{(E_{n+1} - E_n)^2}. \quad (8)$$

In this calculation, one has to evaluate the summation of matrix elements for the current operator \hat{j} such as $\langle n | \hat{j} | n+1 \rangle$ or $\langle n+1 | \hat{j} | n \rangle$, where $|n\rangle$ or $|n+1\rangle$ denotes the states connected by this operator. In the present case of graphite in the quasi-quantum limit, these states should be chosen from the subbands having different Landau indices by the number of 1 and the same wave numbers and spins. Since conductivity is determined by the summation of these matrix elements of the inter-subband transitions over a wide region of the reciprocal space, gap formation at a part of the subband may cause the limited effect on the Hall conductivity in the density-wave state while the gap is considerably smaller than the energy difference in the adjacent subbands. In other words, a comparison between the experimental data of σ_{xy} and such calculations will provide an in-depth evaluation for several models of subband structures above 53 T. We leave it as an open problem because this calculation is beyond the scope of this paper.

In this study, we consider the possible subband structure through a more qualitative argument. Firstly, the observed small ρ_{xy} seems to fit with the symmetric subband structure with respect to the Fermi level, as illustrated in Fig. 1(a), rather than the asymmetric one caused

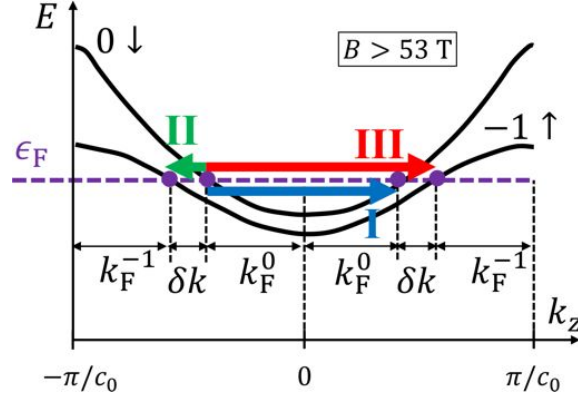


Fig. 6. (Color online) Proposed subband structure realized above 53 T and possible three nesting vectors, labeled I, II, and III.

by the depopulation of the $-1\downarrow$ subband only. Secondly, hole doping increases the distance between the Fermi points in the $-1\downarrow$ subband, as shown in Fig. 1(b), which requires a large field to detach from the Fermi level. On the contrary, our experimental results show smaller transition fields for α' in the neutron-irradiated graphite with a higher hole concentration. Thirdly, the nearly simultaneous depopulation of two subbands seems to be natural from the viewpoint of the charge neutrality condition. Therefore, we interpret the behaviors of Hall resistivity and magnetization as features of the realization of the quantum limit state in which only two subbands (electron-like $0\downarrow$ and hole-like $-1\uparrow$ subbands) cross the Fermi level.

The observed increase in ρ_{zz} above 53 T suggests the emergence of a novel density-wave state between 53 and 75 T in the quantum limit state.¹¹⁾ In this state, the possible nesting vectors are shown in Fig. 6 by arrows labeled I, II, and III. Here, we assume simultaneous nesting between the residual two Fermi points connected by the same wave vector for each state to reproduce the observed insulating behavior, although the nesting vectors are not described in Fig. 6 for clarity. Vector I represents the charge-density-wave phase, whereas the inter-subband nesting with vectors II and III denote the excitonic phase.^{4,5,25,26)} According to the original argument of the excitonic insulator,²⁶⁾ the present gapped state caused by the instability of the Fermi surface can be expressed by the BCS-like formulation and called the excitonic BCS-like state. As stated in Ref. 6, the charge-density-wave phases can be less stable because of the direct Coulomb interaction. Therefore, a gap will be formed at the Fermi energy by the inter-subband nesting with vector II or III, and simultaneously between the residual two Fermi points. Taking into account the charge neutrality condition ($k_F^0 = k_F^{-1}$), the length of vector III ($2k_F^0 + \delta k$) is locked to π/c_0 . We consider that such a commensu-

rate modulation can be more favorable than the incommensurate one characterized by vector Π . In this commensurate state, the carriers in a pair have a finite average momentum, i.e., $(k_F^0 + \delta k) - k_F^0 = \delta k$, analogous to the Fulde-Ferrell-Larkin-Ovchinnikov (FFLO) phase in superconductors.^{27,28)} With increasing magnetic field, the value of $2k_F^0 + \delta k$ remains π/c_0 , whereas δk increases. The reported additional anomaly at 75 T might be a transition induced by increasing δk . The true nature of this transition will be clarified through additional experiments in the future.

4. Conclusions

The transport and magnetic properties of graphite were investigated at pulsed magnetic fields up to 75 T. The Hall resistivity becomes nearly zero as the applied magnetic field approaches 53 T. In addition, an anomaly is observed in differential magnetization at about 53 T. This transition field is reduced by doping holes. These results support the realization of the quantum limit state, where only two subbands (one electron-like and one hole-like spin-polarized subband) cross the Fermi level, in the field region over 53 T. The formation of the density-wave state in this situation can be regarded as the excitonic BCS-like state.

Acknowledgment

We thank Y. Iye for supplying various samples, and T. Osada and Y. Takada for valuable discussion and comments.

References

- 1) J. C. Slonczewski and P. R. Weiss, Phys. Rev. **109**, 272 (1958).
- 2) J. W. McClure, Phys. Rev. **108**, 612 (1957).
- 3) S. Tanuma, R. Inada, A. Furukawa, O. Takahashi, Y. Iye, and Y. Onuki, in *Physics in High Magnetic Fields*, ed. S. Chikazumi and N. Miura (Springer, Berlin, 1981) p. 316.
- 4) Y. Iye, P. M. Tedrow, G. Timp, M. Shayegan, M. S. Dresselhaus, G. Dresselhaus, A. Furukawa, and S. Tanuma, Phys. Rev. B **25**, 5478 (1982).
- 5) D. Yoshioka and H. Fukuyama, J. Phys. Soc. Jpn. **50**, 75 (1980).
- 6) K. Takahashi and Y. Takada, Physica B **201**, 384 (1994).
- 7) H. Yaguchi and J. Singleton, J. Phys.: Condens. Matter **21**, 344207 (2009).
- 8) Y. Takada and H. Goto, J. Phys.: Condens. Matter **10**, 11315 (1998).
- 9) H. Yaguchi and J. Singleton, Phys. Rev. Lett. **81**, 5193 (1998).
- 10) H. Yaguchi, J. Singleton, and T. Iwata, Physica B **298**, 546 (2001).
- 11) B. Fauqué, D. LeBoeuf, B. Vignolle, M. Nardone, C. Proust, and K. Behnia, Phys. Rev. Lett. **110**, 266601 (2013).
- 12) Y. Kopelevich, B. Raquet, M. Goiran, W. Escoffier, R. R. da Silva, J. C. Medina Pantoja, I. A. Luk'yanchuk, A. Sinchenko, and P. Monceau, Phys. Rev. Lett. **103**, 116802 (2009).
- 13) A. Kumar, J. Poumirol, W. Escoffier, M. Goiran, B. Raquet, and J. C. Pivin, J. Phys.: Condens. Matter **22**, 436004 (2010).
- 14) S. Uji, J. S. Brooks, and Y. Iye, Physica B **246**, 299 (1998).
- 15) Y. Iye and G. Dresselhaus, Phys. Rev. Lett. **54**, 1182 (1985).
- 16) H. Yaguchi, T. Takamasu, Y. Iye, and N. Miura, J. Phys. Soc. Jpn. **68**, 181 (1999).
- 17) Q. A. Li, K. E. Gray, and J. F. Mitchell, Phys. Rev. B **59**, 9357 (1999).
- 18) G. A. Levin, J. Appl. Phys. **81**, 714 (1997).
- 19) G. Machel and M. von Ortenberg, Physica B **211**, 355 (1995).
- 20) H. Ochimizu, T. Takamasu, S. Takeyama, S. Sasaki, and N. Miura, Phys. Rev. B **46**, 1986 (1992).
- 21) K. Sugihara and J. A. Woollam, J. Phys. Soc. Jpn. **45**, 1891 (1978).
- 22) H. Yaguchi, Y. Iye, T. Takamasu, N. Miura, and T. Iwata, J. Phys. Soc. Jpn. **68**, 1300 (1999).

- 23) H. Yaguchi and J. Singleton, *J. Phys.: Conf. Ser.* **150**, 022099 (2009).
- 24) Y. Iye, L. E. McNeil, and G. Dresselhaus, *Phys. Rev. B* **30**, 7009 (1984).
- 25) E. W. Fenton, *Phys. Rev.* **170**, 816 (1968).
- 26) D. Jérôme, T. M. Rice, and W. Kohn, *Phys. Rev.* **158**, 462 (1967).
- 27) P. Fulde and R. A. Ferrell, *Phys. Rev.* **135**, A550 (1964).
- 28) A. I. Larkin and Yu. N. Ovchinnikov, *Zh. Eksp. Teor. Fiz.* **47**, 1136 (1964) [translation: *Sov. Phys. JETP* **20**, 762 (1965)].